











The phosphorylated pathway of serine biosynthesis affects sperm, embryo, and sporophyte development, and metabolism in *Marchantia polymorpha*

Mengyao Wang^{1,2}, Hiromitsu Tabeta ^{1,3,4,12}, Kinuka Ohtaka^{1,2,10,12}, Ayuko Kuwahara¹, Ryuichi Nishihama ^{5,11}, Toshiki Ishikawa ⁶, Kiminori Toyooka ¹, Mayuko Sato ¹, Mayumi Wakazaki¹, Hiromichi Akashi¹, Hiroshi Tsugawa ^{1,7}, Tsubasa Shoji¹, Yozo Okazaki^{1,8}, Keisuke Yoshida ⁹, Ryoichi Sato¹, Ali Ferjani ⁴, Takayuki Kohchi ⁵ & Masami Yokota Hirai ^{1,2}✉

Serine metabolism is involved in various biological processes. Here we investigate primary functions of the phosphorylated pathway of serine biosynthesis in a non-vascular plant *Marchantia polymorpha* by analyzing knockout mutants of MpPGDH encoding 3-phosphoglycerate dehydrogenase in this pathway. Growth phenotypes indicate that serine from the phosphorylated pathway in the dark is crucial for thallus growth. Sperm development requires serine from the phosphorylated pathway, while egg formation does not. Functional MpPGDH in the maternal genome is necessary for embryo and sporophyte development. Under high CO₂ where the glycolate pathway of serine biosynthesis is inhibited, suppressed thallus growth of the mutants is not fully recovered by exogenously-supplemented serine, suggesting the importance of serine homeostasis involving the phosphorylated and glycolate pathways. Metabolomic phenotypes indicate that the phosphorylated pathway mainly influences the tricarboxylic acid cycle, the amino acid and nucleotide metabolism, and lipid metabolism. These results indicate the importance of the phosphorylated pathway of serine biosynthesis in the dark, in the development of sperm, embryo, and sporophyte, and metabolism in *M. polymorpha*.

¹RIKEN Center for Sustainable Resource Science, Yokohama, Japan. ²Graduate School of Bioagricultural Sciences, Nagoya University, Nagoya, Japan. ³Graduate School of Arts and Sciences, The University of Tokyo, Tokyo, Japan. ⁴Department of Biology, Tokyo Gakugei University, Tokyo, Japan. ⁵Graduate School of Biostudies, Kyoto University, Kyoto, Japan. ⁶Graduate School of Science and Engineering, Saitama University, Saitama, Japan. ⁷Department of Biotechnology and Life Science, Tokyo University of Agriculture and Technology, Tokyo, Japan. ⁸Graduate School of Bioresource, Mie University, Tsushi, Japan. ⁹Institute of Innovative Research, Tokyo Institute of Technology, Yokohama, Japan. ¹⁰Present address: Department of Chemical and Biological Sciences, Japan Women's University, Tokyo, Japan. ¹¹Present address: Department of Applied Biological Science, Faculty of Science and Technology, Tokyo University of Science, Tokyo, Japan. ¹²These authors contributed equally: Hiromitsu Tabeta, Kinuka Ohtaka. ✉email: masami.hirai@riken.jp

Serine, an amino acid highly accumulated in plants¹, is involved in cell signaling in response to various environmental stresses and the biosynthesis of various biomolecules, such as nitrogenous bases, phospholipids, and sphingolipids^{2–4}. In plants, three serine biosynthesis pathways exist and function coordinately in the daytime. The major pathway during daytime is the photorespiratory glycolate pathway in photosynthetic tissues^{5–7} (Supplementary Fig. 1). In this pathway, glycine decarboxylase complex and serine hydroxymethyltransferase (SHMT) convert glycine to serine^{8,9}. In dark environments and non-photosynthetic tissues, two other pathways are responsible for serine synthesis, namely, the glycerate and phosphorylated pathways^{9,10}.

The glycerate pathway starts with the dephosphorylation of 3-phosphoglycerate (3-PGA) by 3-PGA phosphatase in the cytosol or peroxisomes, followed by a sequence of reactions catalyzed by glycerate dehydrogenase (GDH) and alanine: hydroxypyruvate (serine: pyruvate) aminotransferase^{5,11–13}. On the other hand, the phosphorylated pathway from 3-PGA occurs in plastids and is catalyzed by 3-PGA dehydrogenase (PGDH), 3-phosphoserine aminotransferase (PSAT), and 3-phosphoserine phosphatase (PSP)^{9,14,15}.

The phosphorylated pathway is conserved in animals, plants, and bacteria^{4,16}. This pathway in plants is the only serine source for specific cell types and is essential for the embryo, pollen, male gametophyte, and postembryonic root development in *Arabidopsis thaliana*^{3,17–19}. The phosphorylated pathway of serine biosynthesis (PPSB) has been suggested to play a fundamental role in plant responses to various environmental stresses, such as low temperature, high salinity, and pathogens^{3,4,17,20}. Although the reason why plants take three routes for serine biosynthesis is unclear, serine production through the phosphorylated pathway is crucial in plant metabolism and development^{3,21}. The genes encoding PGDH are important checkpoints in PPSB as they are under tight transcriptional control and responsible for several physiological events³. In *A. thaliana*, three PGDH isoforms (*AtPGDH1*, *AtPGDH2*, and *AtPGDH3*) are expressed in different organs/tissues and have different physiological functions. *AtPGDH1* is the essential gene and its silencing causes developmental arrest in roots, embryos, pollen, and male gametophytes. *AtPGDH2* has a partially redundant role with *AtPGDH1*, while *AtPGDH3* seems to have additional functions unrelated to serine synthesis^{17–19,22,23}. In rice (*Oryza sativa*), three *OsPGDH* genes were expressed in all tissues and development stages, and their expressions responded to abiotic stresses²⁴. Additionally, four *PpPGDHs* and two *AmtrPGDHs* were identified in moss *Physcomitrium patens* and basal angiosperm *Amborella trichopoda*, respectively²⁵. The biochemical properties of various PGDH enzymes are different among isozymes in terms of allosteric regulation by amino acids^{25,26}. Considering that all land plant species examined, except *Marchantia polymorpha* L., possess different types of PGDH isozymes, duplication and functional diversification of the *PGDH* genes was necessary for the evolution of land plants to adequately control the serine supply^{25,27}.

Marchantia polymorpha is a model bryophyte species and a dioecious plant with a haploid genome. *M. polymorpha* is increasingly used as a model plant for physiological, genetic, epigenetic, metabolic, and evolutionary studies. Recent studies have clarified metabolic responses to wounding stress²⁸, cellular expansion and integrity²⁹, reproductive development³⁰, as well as the mechanisms of spermatogenesis and embryogenesis^{31–35}. Our previous study characterized the sole PGDH enzyme, MpPGDH, a 65.6 kDa protein sharing 75–80% identity with *AtPGDHs*²⁷. MpPGDH has similar biochemical characteristics to *AtPGDH1* in vitro, such as cooperative inhibition by L-serine and activation by

L-alanine, L-valine, L-methionine, L-homoserine, and L-homocysteine²⁷.

In this study, we aim to clarify the in vivo function of MpPGDH and explore the specific functions of serine from the phosphorylated pathway in a non-vascular plant *M. polymorpha*. Our results revealed the particular importance of serine from the phosphorylated pathway on vegetative growth, male gametogenesis, and sporophyte development in *M. polymorpha* and that PPSB is involved in the metabolism of the tricarboxylic acid (TCA) cycle, amino acids, nucleotides, and lipids, in a different manner under different light and CO₂ conditions in *M. polymorpha*. This study proposes that serine homeostasis is a key factor for robustness of not only metabolism but also growth and development.

Results

Serine supply from the phosphorylated pathway in the dark is crucial for thallus growth. The expression pattern of MpPGDH was clarified using the *proMpPGDH:GUS* transgenic lines. In vegetative phase, MpPGDH was expressed in almost the entire gemma (Supplementary Fig. 2a) and displayed a linear expression pattern in the midribs from the center of the thallus to the apical notches in 1- to 4-week-old thalli (Supplementary Fig. 2b–d).

The knockout mutants of MpPGDH were generated by introducing the CRISPR/Cas9 constructs into sporelings (Supplementary Fig. 3a). The reduced transcript level of MpPGDH and no detectable level of MpPGDH protein were confirmed in both male and female *Mppgdh* mutants (Supplementary Fig. 3b, c).

Considering that photosynthesis may affect serine biosynthesis in plants, thalli were grown under 16-h light/8-h dark (L/D) and continuous light (CL) conditions for comparison. Under the L/D condition, male *Mppgdh-1* and *Mppgdh-2* lines were significantly small in thallus size and fresh weight (Fig. 1) compared with the wild type. However, the severe growth phenotype of *Mppgdh* mutants was resolved by the exogenously-supplemented serine (Fig. 1). In contrast, no difference was observed between the mutants and wild type under the CL condition, while *M. polymorpha* grew better under this condition than the L/D condition (Fig. 1). Similar growth phenotypes were observed in the female *Mppgdh* knockout mutants (*Mppgdh-3*, *Mppgdh-4*, and *Mppgdh-5*; Supplementary Fig. 4). For further experiments, *Mppgdh-1* and *Mppgdh-3* were used since the supply of serine restored the growth of these mutants to the wild-type levels.

Poor growth phenotype observed only under L/D conditions suggested the importance of the PPSB in the dark. Then, the transcript levels of some key genes involved in three serine biosynthesis pathways were analyzed in the thallus transferred from CL to dark conditions. The expression of MpPGDH and MpPSAT in the PPSB was significantly induced at 8 and 16 h post transfer to darkness, respectively, compared with CL conditions (Supplementary Fig. 5). The MpPGDH and MpSHMT expression levels in the glycerate and glycolate pathways, respectively, were gradually reduced in darkness. These results suggest that the PPSB was enhanced and functioned as the primary serine synthesis pathway under dark conditions.

To determine whether poor growth of the mutant thalli under L/D conditions was attributed to insufficient serine content, free amino acid contents in the thallus were measured. The serine content in *Mppgdh* mutants was significantly decreased after 4 h in the dark and restored to wild type-level after 2 h in the light (Fig. 2). These results suggested that reduced serine content during the dark period caused the poor growth in *Mppgdh* mutants under L/D conditions.

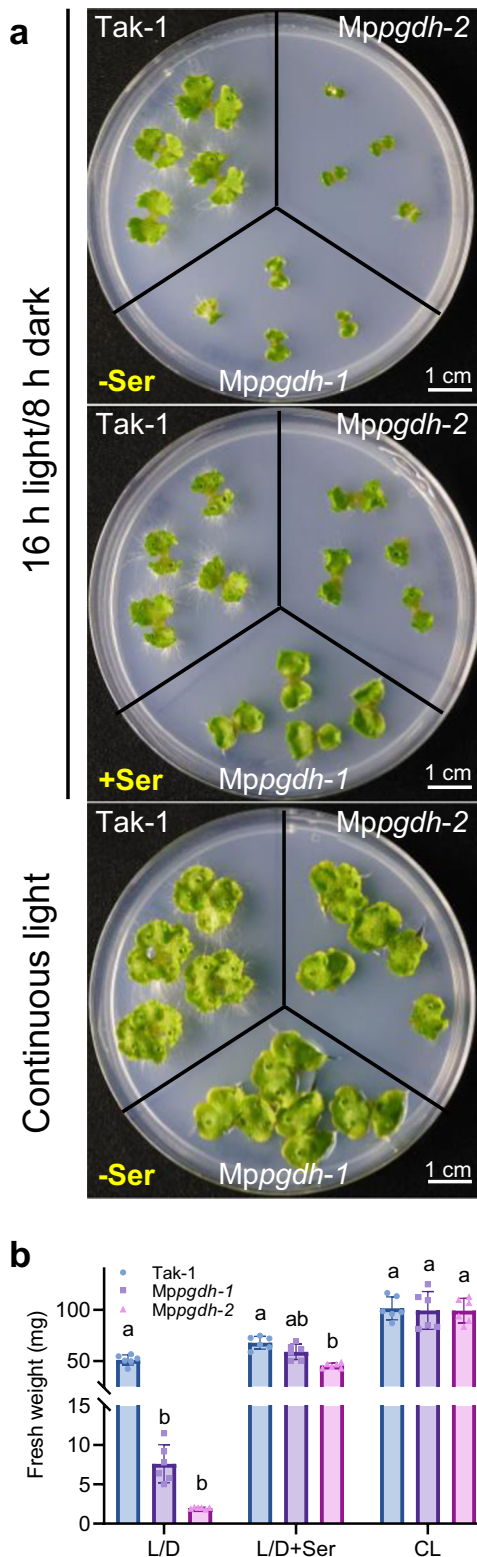


Fig. 1 Thallus growth in the male *Mppgdh* mutants. **a** Plants grown on $\frac{1}{2}$ B5 agar medium for 14 days with or without serine supplementation under 16 h light/8 h dark (L/D) or continuous light (CL) conditions. **b** The fresh weight of *Mppgdh-1*, *Mppgdh-2*, and wild-type Tak-1. Data represent means \pm SD of six biological replicates ($n = 6$). One-way ANOVA followed by Tukey's test ($p < 0.01$) was performed in each group; columns with the same letter are not significantly different.

Overall, these results indicate that the perturbation of the PPSB impaired thallus growth under the L/D condition, revealing the crucial function of PPSB in the dark for thallus growth.

MpPGDH-mediated serine synthesis is essential to sperm development. The growth phenotype of *Mppgdh* mutants was observed in the whole life cycle under the L/D condition to understand the importance of PPSB. The formation of gemma cups and gemmae in the *Mppgdh* mutants was normal, likewise those of wild types (Supplementary Fig. 6).

The male *Mppgdh* mutants developed umbrellalike antheridiophores (male reproductive branch) under far red-supplemented long-day conditions, which induce sexual reproduction in wild type (Fig. 3a, b). Antheridiophore development is generally divided into five stages (Supplementary Fig. 7a)³⁶. When water was dropped on the dorsal surface of the antheridiophores at stage 4, white sperm masses discharged from antheridia emerged through the antheridial pores in wild type (Fig. 3c). Notably, no white sperm mass was observed in the *Mppgdh* mutants after water application (Fig. 3c and Supplementary Fig. 7b). When cells in water were visualized via fluorescence staining of DNA, sperm with thin and crescent-shaped nucleus were visible, and very few sperm cells were observed in the *Mppgdh-1* compared with wild-type Tak-1 (Fig. 3d).

To ascertain which process of sperm development (Fig. 3e) was impaired in the *Mppgdh* mutants, the sections of resin-embedded antheridia were analyzed using field emission scanning electron microscopy (FE-SEM) at the early-, middle-, and mature stages. In wild-type Tak-1, spermatid mother cells were rectangular (Fig. 3f, top left) and underwent diagonal cell division to produce spermatids (Fig. 3f, top middle). In the spermatid stage, flagellar formation was observed. Lastly, the spermatids differentiated into sperm cells (Fig. 3f, top right). However, in the *Mppgdh* mutants, spermatid mother cells were in various sizes and irregular shapes (Fig. 3f, bottom left), and subsequent diagonal cell division to generate spermatids was barely observed (Fig. 3f, bottom middle and right). The qRT-PCR analysis of sperm differentiation-related genes (Supplementary Fig. 8) revealed that the expression of *MpPRM*, which is expressed specifically in sperm during late spermiogenesis³⁷, were significantly repressed. On the other hand, the expression level of *MpDUO1*, which is an upstream regulator of *MpPRM* and expressed in spermatid mother cells and spermatids³⁶, was similar in the wild type and the mutants. These results support the notion that cell division of spermatid mother cells to generate spermatids was blocked in the *Mppgdh* mutants.

The GUS staining of the male *proMpPGDH::GUS* lines indicated that *MpPGDH* was expressed in the middle area of antheridial receptacles (Supplementary Fig. 2e). Analysis using the Expression Database for *M. polymorpha*³⁷ confirmed that *MpPGDH* is expressed in antheridia (Supplementary Fig. 2g).

To clarify whether exogenous serine supplementation and continuous light conditions rescue the defective spermatogenesis phenotype, the mutants grown under L/D + serine conditions and CL conditions were microscopically observed. Under these two conditions, the phenotype of *Mppgdh* mutants was partially rescued (Supplementary Fig. 7c–f). Sperm masses were discharged in the *Mppgdh* mutants (Supplementary Fig. 7c, e), but fewer sperm cells were observed compared with wild type (Supplementary Fig. 7d, f). The FE-SEM images indicated that the cell division of spermatid mother cells in *Mppgdh-1* was rescued to some extent by serine supplement and CL, since diagonal cell divisions were visible in some regions in one antheridium (Supplementary Fig. 7g, h). The borders between the areas comprising cells in different states were clearly observed (Supplementary Fig. 7g, h), suggesting that

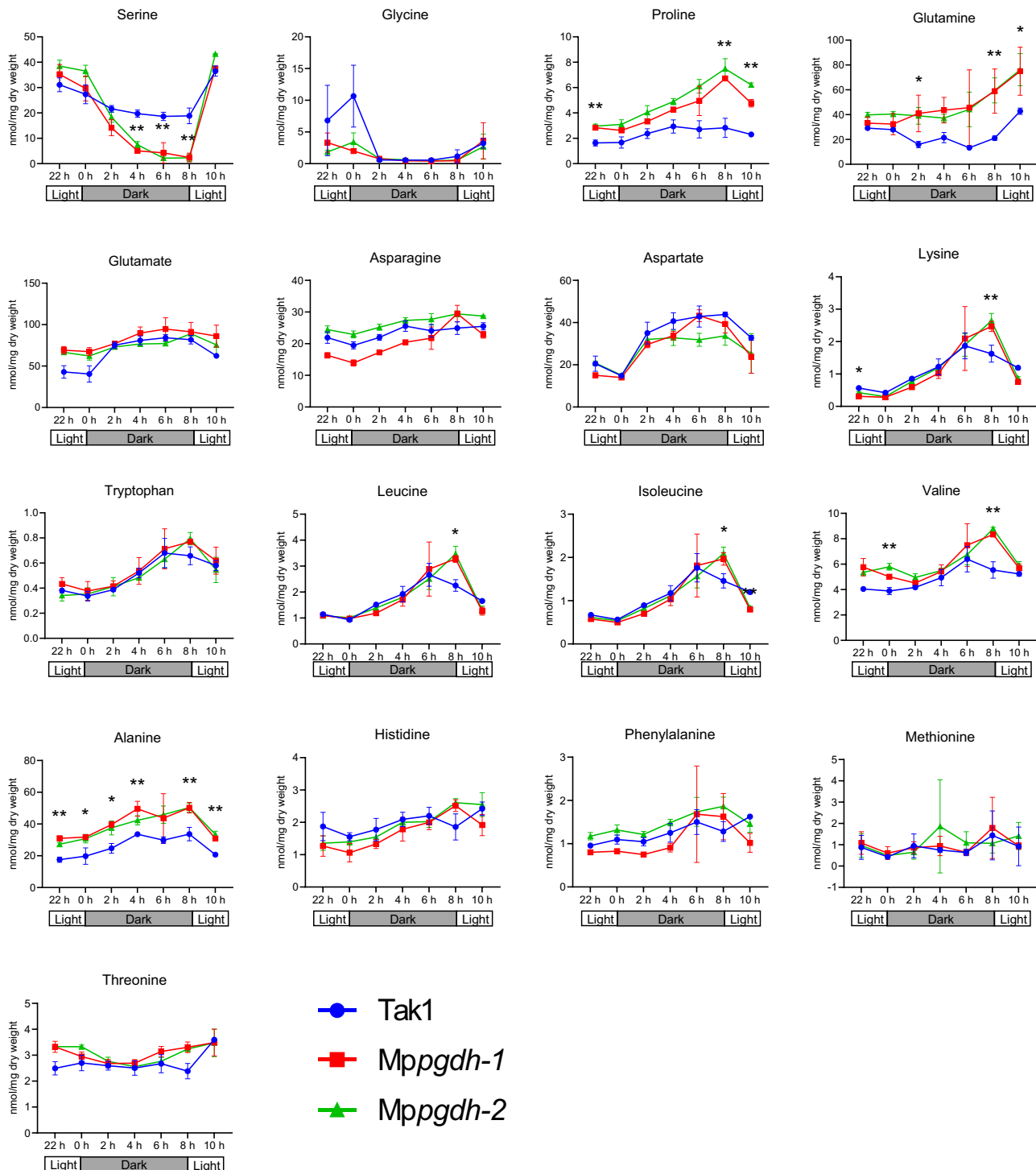


Fig. 2 Free amino acid contents in thalli of the *Mppgdh* mutants under L/D conditions. The thalli of male lines grown under 16 h light/8 h dark conditions were sampled at 0 h, 2 h, 4 h, 6 h, and 8 h in the dark period, and at 2 h and 14 h in the light period. The free amino acid contents were measured using gas chromatography–quadrupole mass spectrometry. Data represent means \pm SD of three biological replicates. Student's *t*-test was performed between wild type and one mutant respectively. Asterisks indicate statistically significant differences between the wild type and both two mutant lines (* p < 0.05, ** p < 0.01).

groups of neighboring cells in one antheridium share a similar status in terms of serine supply in *Mppgdh-1*. Partial recovery by exogenous serine supplement and CL conditions may result in fewer number of sperm cells per antheridium in the mutants compared with the wild type.

In the female *Mppgdh* mutants, no apparent morphological differences were observed in the formation of archegoniophores

(female reproductive branch, Fig. 4a, b) and archegonia (Fig. 4c) under the L/D condition supplemented with far-red light, compared with that in the wild type. Analysis using the Expression Database for *M. polymorpha* indicated that *MpPGDH* is expressed in archegoniophore and archegonium (Supplementary Fig. 2g).

These results suggest that male gametogenesis required serine supply from the phosphorylated pathway.

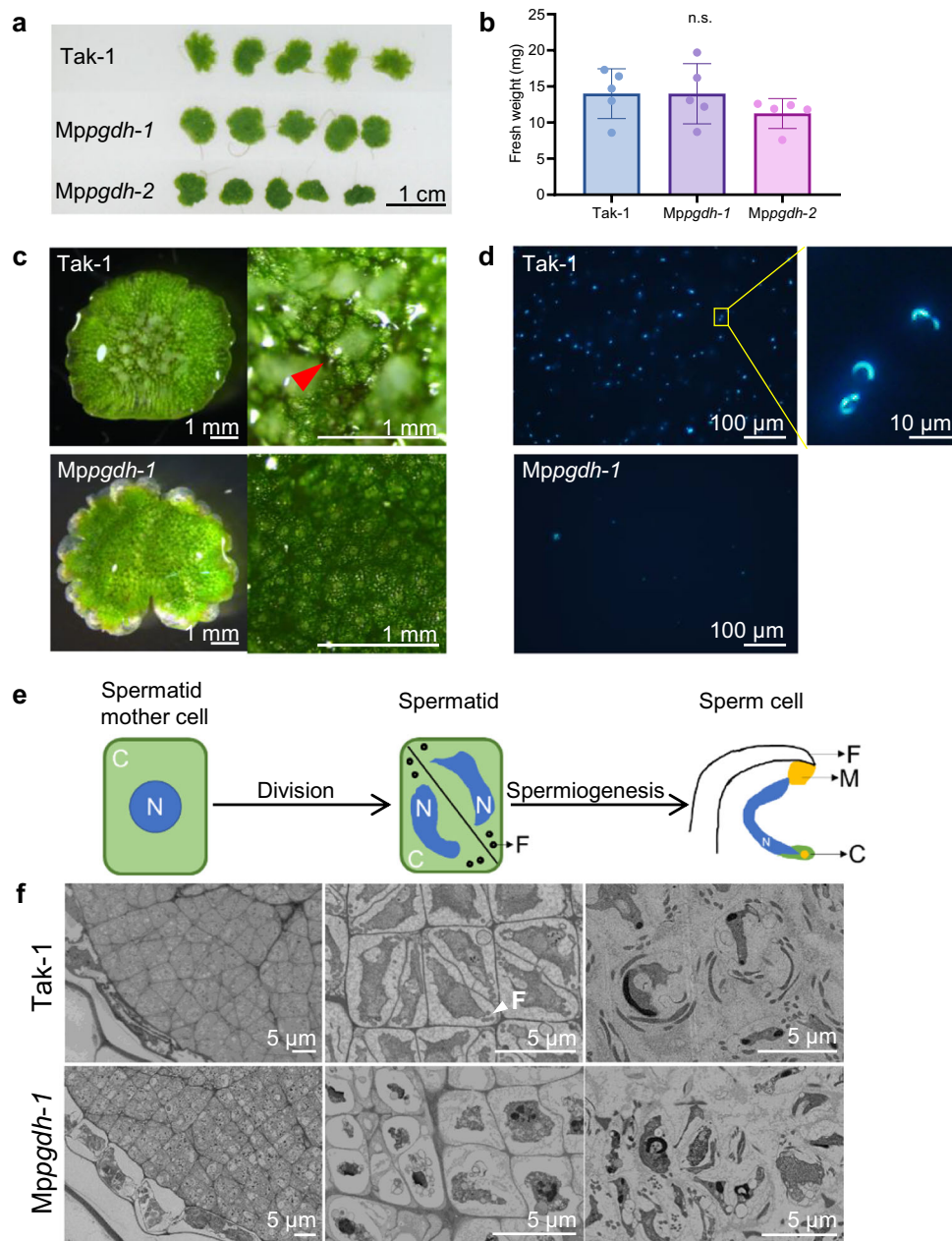


Fig. 3 Male gametogenesis in the *Mppgdh* mutants. **a** Images of antheridial receptacles of Tak-1, *Mppgdh-1*, and *Mppgdh-2* grown under L/D conditions. **b** The fresh weight of antheridial receptacles in **(a)**. Data represent means \pm SD of five biological replicates ($n = 5$). One-way ANOVA followed by Tukey's test ($p < 0.05$) was performed (n.s., no significant difference). **c** Discharge of sperm masses. The white sperm masses (red arrowhead) were visible 10 min after dropping 50 μ L water on the dorsal surface of antheridial receptacles. **d** Fluorescent staining of the cells. The cells in 10 μ L water taken from **(c)** were visualized via Hoechst staining. Nuclei of sperm were very thin and crescent-shaped. **e** Schematic diagram of sperm development in wild type. **f** Field emission scanning electron microscopy (FE-SEM) images showing the process of *M. polymorpha* male gamete development. Cells in an early-stage antheridium (left), a middle-stage antheridium (middle), and a mature antheridium (right) are shown. The white arrowhead indicates the flagella. C cytoplasm, N nucleus, F flagella, M mitochondria.

Knockout of MpPGDH in maternal genome affects sporophyte development. We observed the process on the archegoniophore of wild-type Tak-2 and *Mppgdh-3* after fertilization with sperm from wild-type Tak-1. In the Tak-2 x Tak-1 cross, yellow spores were generated and released from sporangia (Fig. 5a), whereas in the *Mppgdh-3* x Tak-1 cross, only empty involucre were developed (Fig. 5b). Cross-sectional images of the developing sporophyte show the detailed process of embryogenesis and sporophyte development post fertilization (Fig. 5c–h). At 1-week post fertilization, a young sporophyte circularly surrounded by a calyptra and pseudoperianth was observed in both Tak-2 x Tak-1

(Fig. 5c) and *Mppgdh-3* x Tak-1 (Fig. 5d), indicating that fertilization successfully occurred in *Mppgdh-3* x Tak-1 as well. However, a clear delay in embryogenesis was observed in *Mppgdh-3* x Tak-1. In Tak-2 x Tak-1, sporophytes detached into the inner space of the capsule, and differentiation along the apical-basal axis into foot, seta, and sporangium, where sporogenous cells began to differentiate, was clearly evident at 2-week post fertilization (Fig. 5e). At 3-week post fertilization, sporocytes underwent meiosis to produce spores in Tak-2 x Tak-1 (Fig. 5g). In contrast, sporophyte development seemed arrested before the stage of apical-basal differentiation in *Mppgdh-3* x Tak-1 (Fig. 5f, h),

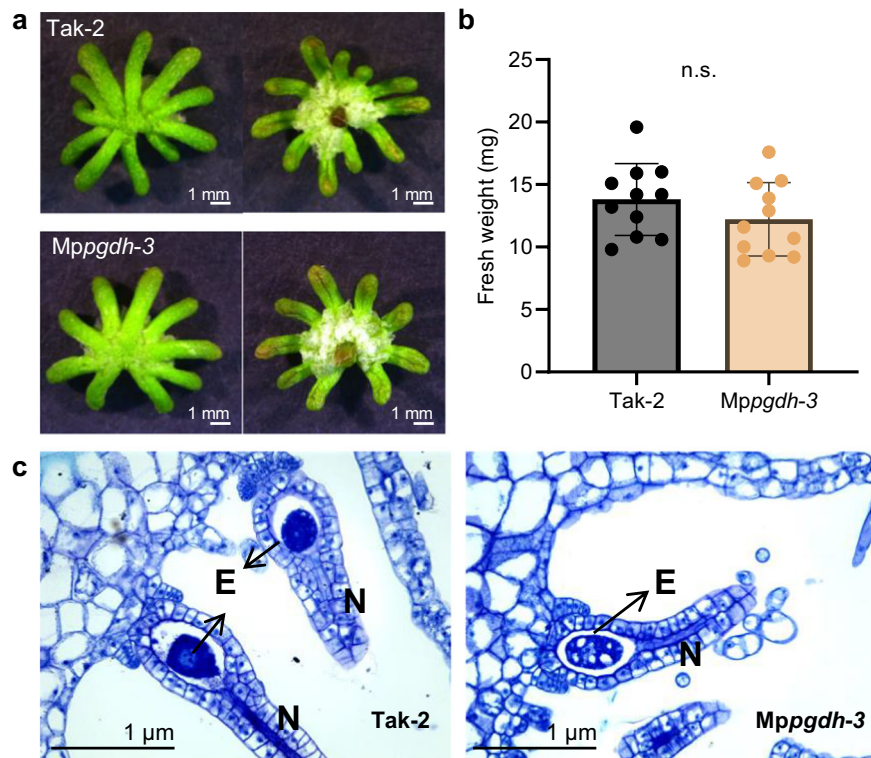


Fig. 4 Oogenesis in the *Mppgdh* mutants. a Images of the archegonial receptacles of Tak-2 and *Mppgdh-3* grown under L/D condition. **b** The fresh weight of archegonial receptacles of Tak-2 and *Mppgdh-3*. Data represent means \pm SD of 11 biological replicates ($n = 11$). Student's *t*-test was performed ($p < 0.05$, n.s., no significant difference). **c** The cross-section images of archegonia. E egg cell, N neck.

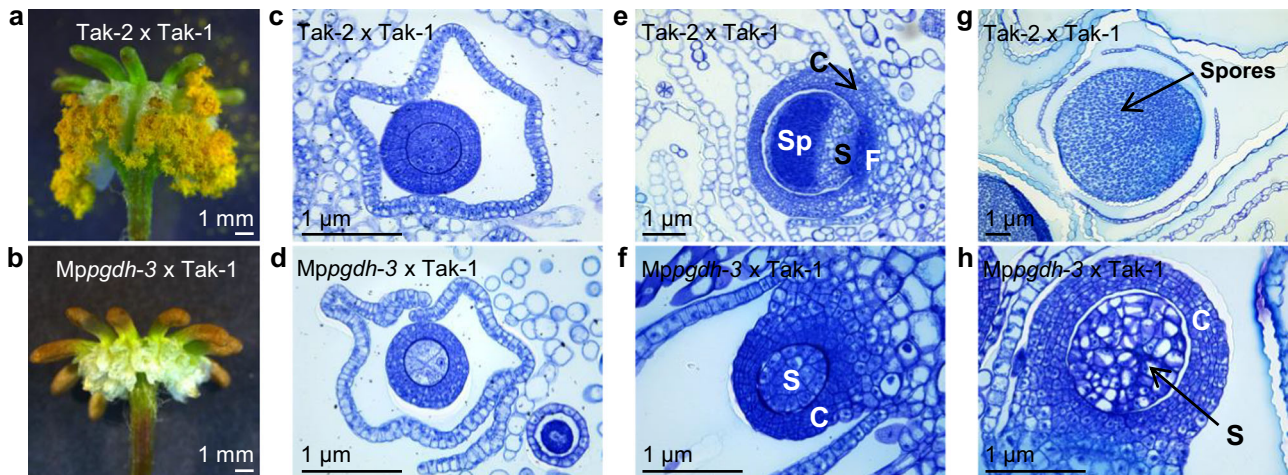


Fig. 5 Sporulation in the female *Mppgdh* mutant following fertilization with sperm from the wild type. a, b The sporulation on Tak-2 (a) and *Mppgdh-3* (b) approximately 1-month post fertilization with sperm from Tak-1. Images are representative of three archegoniophores. (c–h) The cross-section images of sporophytes at 1-week (c, d), 2-week (e, f), and 3-week (g, h) post fertilization. Tak-2 x Tak-1 (c, e, g), *Mppgdh-3* x Tak-1 (d, f, h). C calyptra, F foot, S seta, Sp sporangium.

resulting in no spore production. Considering that paternal chromosomes are repressed during throughout embryogenesis (diploid phase)³⁵, this phenotype was attributed to the lack of the functional *MpPGDH* in maternal genome. Interestingly, according to the Expression Database for *M. polymorpha*, the strongest expression of *MpPGDH* was observed in sporophyte (Supplementary Fig. 2g). Under the CL conditions, the *Mppgdh-3* x Tak-1 zygotes produced spore-bearing structures, and these spores germinated and grew into healthy individuals (Supplementary Fig. 9).

These results indicate that the knockout of *MpPGDH* gene in maternal genome affected embryo and sporophyte development after fertilization.

***MpPGDH* knockout affects amino acid and nucleotide metabolism and the TCA cycle.** To determine how *MpPGDH* knockout affects metabolism, we performed a widely targeted metabolome analysis.

The *Mppgdh* mutants were grown under the L/D, CL, and L/D + serine conditions, and the metabolome in thalli was analyzed

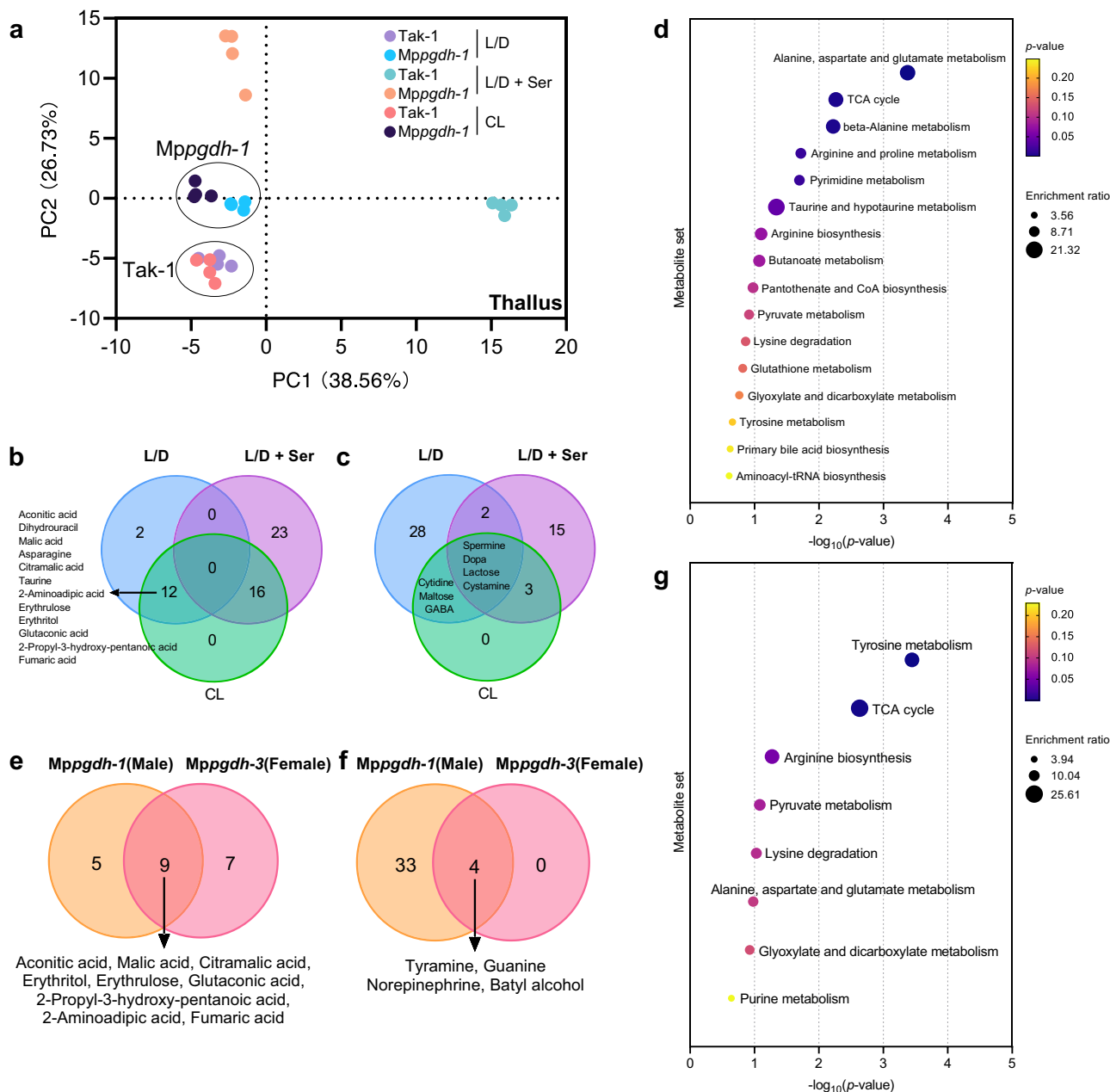


Fig. 6 Changes in metabolome in 14-day-old thalli of the *Mppgdh* mutants. **a** PCA score plot of Tak-1 and *Mppgdh-1* thallus samples grown under L/D, L/D + serine, and CL conditions ($n = 4$). **b, c** Venn diagrams showing the number of significantly decreased metabolites (**b**) and increased metabolites (**c**) in thalli of *Mppgdh-1*. **d** KEGG pathway enrichment of common DAMs under L/D and CL conditions shown in (**b, c**). **e, f** Venn diagrams showing the number of significantly decreased metabolites (**e**) and increased metabolites (**f**) in thalli of *Mppgdh-1* and *Mppgdh-3* under L/D conditions. **g** KEGG pathway enrichment analysis of common DAMs shown in (**e, f**). In (**d, g**), vertical and horizontal axes indicate the metabolite set and the value of $-\log_{10}(p\text{-value})$, respectively. The bubble size corresponds to the enrichment ratio. The color bar indicates the corrected p -value; yellow and navy blue represent higher and lower values, respectively. Dopa, 3,4-dihydroxyphenylalanine; GABA, γ -aminobutyric acid.

(Supplementary Fig. 10a). The principal component analysis (PCA) showed that the light condition did not greatly affect the metabolism of wide-type Tak-1 (Fig. 6a). In the PCA score plot, *Mppgdh-1* formed the clusters separated from those of Tak-1 not only under L/D condition but also under CL condition, indicating that the PPSB also works at daytime. The metabolomes of Tak-1 and *Mppgdh-1* supplemented with serine were clearly separated from the others, indicating that abundant serine supplement greatly affected the metabolism in the wild type and mutant in a different manner (Fig. 6a). Similarly, serine supplementation greatly affected the metabolome of the female lines, while the

wild-type Tak-2 and *Mppgdh-3* were not separated in the PCA score plot under L/D and CL conditions without serine supplementation (Supplementary Fig. 11a). Thus, we mainly focused on the differentially accumulated metabolites (DAMs) under L/D and CL conditions in the following analyses. All the DAMs are listed in Supplementary Data 1.

The Venn diagrams (Fig. 6b, c) and volcano plots (Supplementary Fig. 10b, c) show that 12 DAMs were decreased in *Mppgdh-1* commonly under L/D and CL conditions (Fig. 6b), while 7 DAMs were commonly increased under the two conditions (Fig. 6c). The Kyoto Encyclopedia of Genes and

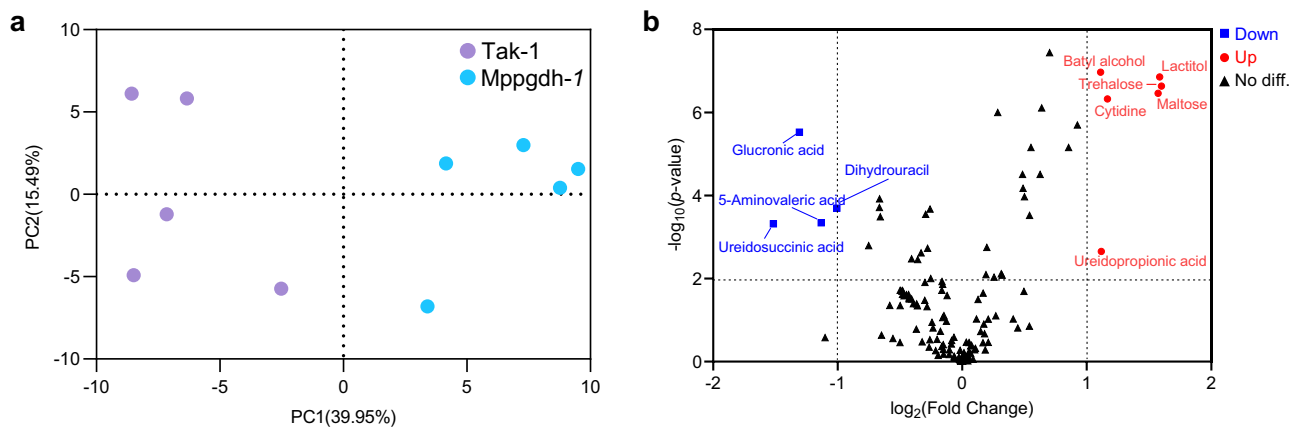


Fig. 7 Changes in metabolome in antheridial receptacles of *Mppgdh-1*. **a** PCA score plot of the antheridial receptacle (stage 4) samples grown under L/D conditions ($n = 5$). **b** Volcano plot showing the DAMs in antheridial receptacles of *Mppgdh-1*. Red dots and blue squares represent significantly increased (p -value < 0.01 , fold change > 2) and decreased (p -value < 0.01 , fold change < 0.5) metabolites, respectively, in *Mppgdh-1*. Black triangles represent no significant differences between Tak-1 and *Mppgdh-1*.

Genomes (KEGG) pathway analysis indicated that these DAMs were significantly enriched ($p < 0.01$) in “alanine, aspartate, and glutamate metabolism,” “TCA cycle,” and “beta-alanine metabolism” (Fig. 6d).

Similarly, DAMs in the female mutant *Mppgdh-3* were analyzed (Supplementary Fig. 11b, c). Under the CL condition, metabolic profiles of *Mppgdh-3* were restored nearly to wild-type level, although the serine content was still significantly reduced in *Mppgdh-3* (Supplementary Fig. 11c). Focusing on common DAMs in *Mppgdh-1* and *Mppgdh-3* under L/D conditions, 9 metabolites decreased (Figs. 6e), and 4 metabolites (Fig. 6f) increased. These DAMs were enriched in “tyrosine metabolism” and “TCA cycle” (Fig. 6g).

We also analyzed metabolome of antheridial receptacles grown under L/D conditions, as *Mppgdh-1* showed severe defect in spermatogenesis under this condition. The *Mppgdh-1* and Tak-1 were separated in the PCA score plot (Fig. 7a), although metabolic profiles fluctuated slightly among replicate samples possibly due to the difficulty in clearly distinguishing antheridiophores at stages 3 or 4 when sampled (Supplementary Fig. 12a). The volcano plot (Fig. 7b) indicates 6 increased metabolites and 4 decreased metabolites, of which lactitol, trehalose, maltose, batyl alcohol, cytidine, and dihydrouracil were common DAMs in thalli and antheridial receptacles.

These results indicate that MpPGDH knockout caused a metabolic change in the thallus and antheridiophore. Lack of functional MpPGDH mainly affected the TCA cycle and amino acid metabolism. Metabolism was affected even under the CL condition, where the *Mppgdh* mutants did not show a visible vegetative phenotype.

MpPGDH knockout alters lipid profiles. Since serine is a precursor of various lipid species, we analyzed the lipidome in the *Mppgdh* mutants.

The lipidome in thalli of the *Mppgdh* mutants grown under the L/D, CL, and L/D + serine conditions were analyzed. In the PCA score plot (Fig. 8a, b), wild types and *Mppgdh* mutants were clearly separated under L/D and CL conditions, indicating a large difference in lipid profiles. Like the metabolic profiles, exogenous serine supplements greatly influenced the lipidome (Fig. 8a, b). Focusing on the differentially accumulated lipid classes (DALCs) (Supplementary Fig. 13), the Venn diagrams showed that lysodiacylglyceryl trimethylhomoserine (LDGTS) and stigmatsterol esters (STSE) decreased under CL conditions (Fig. 8c), while

sitosterol esters (SISE) increased under L/D conditions (Fig. 8d), commonly in male and female thalli. All the DALCs are listed in Supplementary Data 1.

Lipidome of antheridial receptacles grown under L/D conditions was also analyzed (Supplementary Fig. 12b). In the PCA score plot (Fig. 8e), *Mppgdh-1* and Tak-1 were separated from each other. Triacylglycerols (TG), oxidized triglycerides (OxTG), and phosphatidylethanolamines (PE) were present in high amounts, whereas oxidized phosphatidylcholines (OxPC) was present in low amounts in *Mppgdh-1* compared with that in Tak-1 (Fig. 8f).

These results suggest that MpPGDH knockout greatly influenced lipid composition in vegetative and reproductive growth phases of *M. polymorpha*.

PPSB is the primary serine synthesis pathway when photorespiration is inhibited. To estimate the importance of the glycolate pathway on growth and metabolism, the wild types and mutants were grown under L/D conditions in high CO_2 (3000 ppm), which inhibited the glycolate pathway by suppressing photorespiration. GUS staining of *proMpPGDH::GUS* line showed a strong GUS signal in almost the entire thalli (Supplementary Fig. 2f), indicating that the MpPGDH expression was induced under high CO_2 .

Thalli growth of the mutant was significantly suppressed under high CO_2 (Fig. 9a, b for males; Supplementary Fig. 14a, b for females), while high CO_2 increased the fresh weight of 14-day-old thalli in both wild types and the mutants, probably due to enhanced photosynthesis. When serine was exogenously supplemented, suppressed growth of the mutants was recovered to some extent. However, the fresh weights of the mutants remained significantly lower than those of the wild type. The serine content in *Mppgdh-1* under high CO_2 + serine conditions was approximately 70 nmol/mg DW, which was 3.5-fold higher than that in Tak-1 under high CO_2 conditions without serine supplementation (Supplementary Figure 15). Nevertheless, the *Mppgdh-1* mutant under high CO_2 + serine conditions (approximately 100 mg FW, Fig. 9b) did not grow bigger than the wild type without serine supplementation (approximately 130 mg FW, Fig. 9b). This indicates that thallus growth did not depend only on total serine amount.

Reproductive growth was further observed under high CO_2 . Wild types grew into maturity with healthy reproductive branches in about two months with far-red light, while both

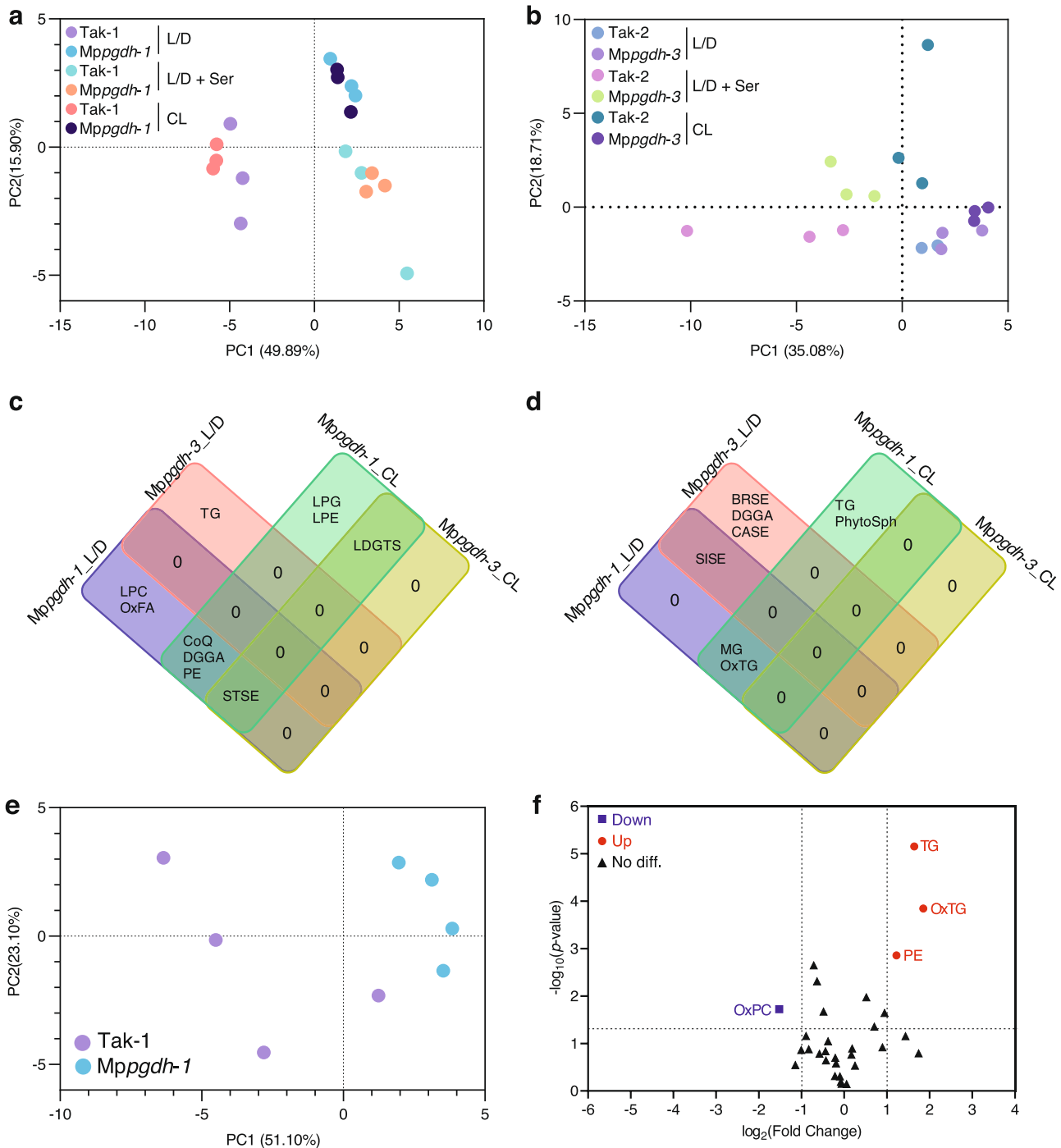


Fig. 8 Changes in lipidome in the *Mppgdh* mutants. **a, b** PCA score plots of male (**a**) and female (**b**) 14-day thallus samples grown under L/D, L/D + serine, and CL conditions ($n = 3$). **c, d** Venn diagrams showing the significantly decreased (**c**) and increased (**d**) lipid classes in thalli of *Mppgdh-1* and *Mppgdh-3* under L/D and CL conditions. **e** PCA score plot of the antheridial receptacle samples grown under L/D conditions ($n = 4$). **f** Volcano plot showing the DALCs in antheridial receptacles of *Mppgdh-1*. Red dots and blue squares represent significantly increased ($p\text{-value} < 0.05$, fold change > 2) and decreased ($p\text{-value} < 0.05$, fold change < 0.5) lipid classes, respectively, in *Mppgdh-1*. Black triangles represent no significant differences between Tak-1 and *Mppgdh-1*. TG triacylglycerol, OxTG oxidized triglyceride, LPG lysophosphatidylglycerol, LPC lysophosphatidylcholine, PE phosphatidylethanolamine, LPE lysophosphatidylethanolamine, LDGTS lysodiacylglyceryl trimethylhomoserine/Lysodiacylglyceryl hydroxymethyl-*N,N,N*-trimethyl- β -alanine, OxFA oxidized fatty acid, CoQ coenzyme Q, DGGGA diacylglyceryl glucuronide, STSE stigmasterol ester, SISE sitosterol ester, BRSE brassicasterol ester, CASE campesterol ester, MG monoacylglycerol, PhytoSph phytosphingosine, OxPC oxidized phosphatidylcholine.

male and female mutants were strongly impaired in growth and did not develop reproductive branches (Supplementary Fig. 16a). Interestingly, exogenous serine supplementation restored reproductive branch formation in *Mppgdh* mutants (Supplementary Fig. 16a), while spermatogenesis was not fully restored

(Supplementary Fig. 16b). Considering that *Mppgdh* mutants developed reproductive branches under L/D and ambient CO_2 conditions but failed in sperm development (Figs. 3a and 4a), the result indicated that enough serine supply from either the glycolate pathway or the PPSB is sufficient for reproductive

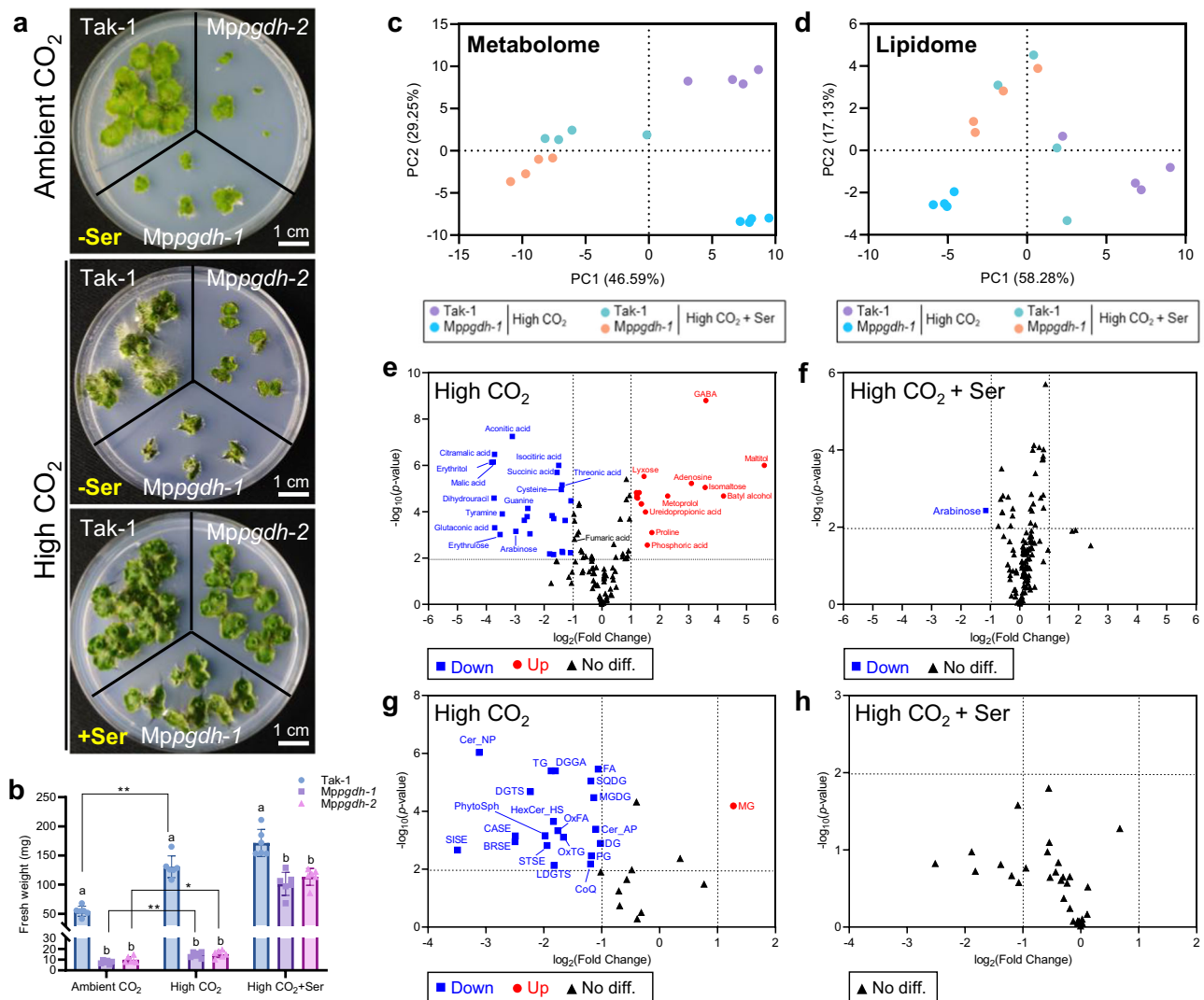


Fig. 9 Growth and metabolic phenotypes of male *Mppgdh* mutants under high CO_2 conditions. **a** Plants grown on $\frac{1}{2}$ B5 agar medium for 14 days under L/D conditions in ambient CO_2 (400 ppm) or high CO_2 (3000 ppm) with or without serine supplementation. **b** The fresh weight of Tak-1 and *Mppgdh* mutants. Data represent means \pm SD of six biological replicates ($n = 6$). One-way ANOVA followed by Tukey's test was performed ($p < 0.05$) in each growth condition; columns with the same letter indicate no significant differences. Student's *t*-test was performed in each line grown under ambient CO_2 and high CO_2 conditions. Asterisks indicate statistically significant differences (Student's *t*-test, * $p < 0.05$, ** $p < 0.01$). **c, d** PCA score plots of the metabolome (**c**) and lipidome data (**d**) in 14-day-old thalli of Tak-1 and *Mppgdh-1* grown under high CO_2 conditions with or without serine supplementation ($n = 4$). **e-h** Volcano plots showing DAMs (**e, f**) and DALCs (**g, h**) in *Mppgdh-1* under the two growth conditions. Red dots and blue squares represent significantly increased (p -value < 0.01 , fold change > 2) and decreased (p -value < 0.01 , fold change < 0.5) metabolites or lipid classes, respectively, in *Mppgdh-1*. Black triangles represent no significant differences between Tak-1 and *Mppgdh-1*.

branch development, while the PPSB is necessary to normal spermatogenesis in *M. polymorpha*.

Metabolism in vegetative growth under high CO_2 was also investigated using metabolome and lipidome analyses. The PCA score plots (Fig. 9c, d) indicate that the metabolic and lipid profiles of *Mppgdh-1* were apparently different from those of Tak-1 under high CO_2 conditions, and the difference between *Mppgdh-1* and Tak-1 became smaller when serine was exogenously supplemented. The volcano plots (Fig. 9e–h) show that high CO_2 affected the accumulation of several metabolites and lipid classes in *Mppgdh-1*, and such perturbed metabolic status was restored by exogenous serine supplementation. A similar trend was observed for *Mppgdh-3* and Tak-2 (Supplementary Fig. 14c–h).

The metabolites and lipid classes whose accumulation were significantly affected by high CO_2 and *MpPGDH* knockout were identified via Venn diagrams. A total of 15 DAMs decreased (Supplementary Fig. 17a), while 3 increased (Supplementary

Fig. 17b) commonly in male *Mppgdh-1* and female *Mppgdh-3*. The KEGG pathway analysis indicates that these DAMs were enriched ($p < 0.01$) in the metabolite sets “TCA cycle,” “butanoate metabolism,” “alanine, aspartate and glutamate metabolism” (Supplementary Fig. 17c). In the case of lipidome, 15 DALCs decreased in male and female mutants under high CO_2 conditions (Supplementary Fig. 17d), while no lipid class was commonly increased. Decreased DALCs included serine-derived lipid classes, such as ceramide alpha-hydroxy fatty acid-phytospingosine (Cer_AP), hexosylceramide hydroxyfatty acid-sphingosine (HexCer_HS).

Discussion

In plants, among three serine biosynthesis pathways, the photorespiratory glycolate pathway is the primary producer of serine during the day⁸. *MpPGDH* expression was induced when thallus

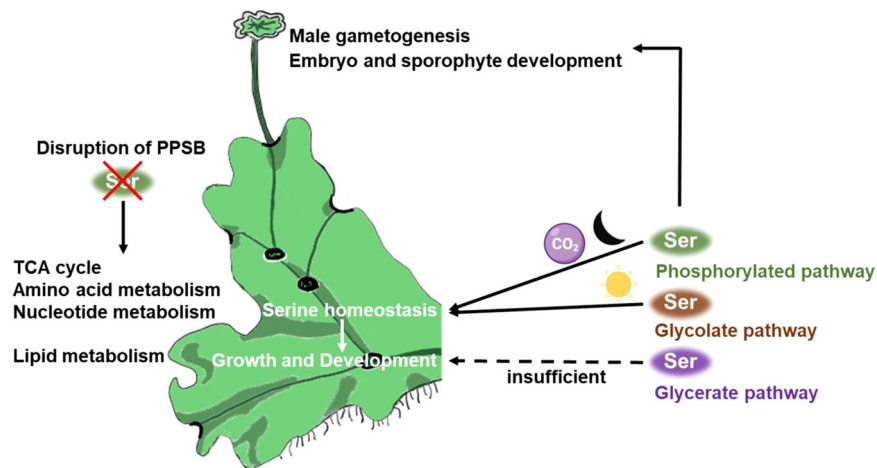


Fig. 10 Proposed model of serine homeostasis in *M. polymorpha*. In *M. polymorpha*, three pathways are involved in serine synthesis. The phosphorylated pathway is the primary serine synthesis pathway when the glycolate pathway is inactive in the dark or under high CO₂ conditions. The phosphorylated and glycolate pathways maintain stability in vivo serine homeostasis for normal growth and development. The phosphorylated pathway plays a unique role in male gametogenesis and embryo and sporophyte development. Disruption of the phosphorylated pathway of serine biosynthesis (PPSB) causes metabolic disorders. The existence and function of the glycerate pathway remain unclear (dashed line).

was transferred to darkness (Supplementary Fig. 5) and grown under high CO₂ conditions (Supplementary Fig. 2f), suggesting a mechanism to activate the PPSB in situations where serine synthesis by the glycolate pathway is suppressed. Consistent with this, the suppressed growth of *Mppgdh* mutants was specifically observed under L/D conditions (Fig. 1 and Supplementary Fig. 4). Furthermore, the serine content in *Mppgdh* mutants was strongly reduced during the dark period and rapidly restored to wild-type level under light (Fig. 2). This indicates that the decreased serine supply during the dark period caused poor growth of *Mppgdh* mutants under L/D conditions. Under CL conditions, serine was continuously synthesized from the glycolate pathway, which was sufficient for growth of the *Mppgdh* mutants (Fig. 1). These results further suggest that stable serine production throughout the day is necessary for vegetative growth.

The *Mppgdh* mutants and the wild type grew better and appeared darker green under high CO₂ (3000 ppm) than under ambient CO₂ (Fig. 9a, b and Supplementary Fig. 14a, b), probably due to enhanced photosynthesis under high CO₂. This result was in contrast to a study using *A. thaliana*, in which elevated CO₂ (4000 ppm) improved the biomass of the wild type but not *AtPGDH1* silencing lines³⁸. The optimal CO₂ concentration for growth may vary depending on plant species and environmental factors such as nutrient availability and light intensity. Under ambient CO₂, the *Mppgdh* mutants continued to grow very slowly, but eventually reached a size comparable to that of the wild type. On the other hand, under high CO₂, the mutant hardly grew further and exogenous serine supplementation did not promote thalli growth in the mutants as much as in the wild type. This indicated that serine is a limiting factor for growth under high CO₂ conditions, but metabolic homeostasis is crucial. Even wild type grew slower and produced fewer sperm under elevated CO₂ than under ambient CO₂ (Supplementary Fig. 16), suggesting high CO₂ widely affects metabolism and other limiting factors than serine for growth and development in *M. polymorpha* also exist under this condition.

Regarding gametogenesis, *Mppgdh-1* barely produced sperm cells under L/D conditions (Fig. 3c, d). Most cells were arrested at the spermatid mother cell stage in the mutants (Fig. 3f). *Mppgdh-1* produced a certain number of sperm cells when supplemented with serine or grown under CL conditions (Supplementary Fig. 7c–f). Zimmermann et al³⁸ proposed that externally supplied

amino acids are metabolized similarly to those produced in plants. In our study, however, exogenously supplemented serine recuperated stagnant thallus growth but did not impair spermatogenesis in *Mppgdh-1*. One possibility is that serine supplied by the PPSB is essential for sperm formation. Another possible reason is that exogenously supplemented serine is not fully transported to the organ/tissue where serine is required. The long-distance transport of serine to the antheridial receptacles or serine translocation from the synthesis site toward the demanding antheridium might be insufficient to support normal developmental processes. It remains unclear whether gametophyte of *M. polymorpha* have photosynthesis-conducting cells³⁹. Detailed spatiotemporal analysis of amino acid contents would provide insights into the importance of serine homeostasis in development. It is interesting to note that mutants in which spermatogenesis is arrested at the spermatid mother cell stage are hitherto unknown. Loss of *MpDUO1*, which is expressed in spermatid mother cells, does not affect its division³¹. Further *Mppgdh* analyses may provide hints for understanding cell division of spermatid mother cell to form spermatid.

Under L/D + high CO₂ conditions, wild types developed reproductive branches, while the growth of *Mppgdh* mutants was arrested at a particular phase (Supplementary Fig. 16a). These findings suggest that serine supply only from the glycerate pathway, the possible third pathway of serine synthesis, is insufficient to maintain the sustained growth of *M. polymorpha*. To date, the existence of the glycerate pathway has been proven by genomic information; however, its function remains elusive. Further studies on this pathway will provide more information on serine homeostasis in plants.

Sexual reproduction is an important developmental process for plants throughout their life cycle. In *A. thaliana*, *AtPSP1*- and *AtPGDH1*-knockout lines showed drastic impairment of pollen development and were sterile^{17–19}, indicating the importance of PPSB in pollen development. In a dioecious plant *M. polymorpha*, although the male *Mppgdh* mutants developed antheridiophores, sperm development was strongly impaired (Fig. 3a–d). After fertilization with wild-type sperm, sporophyte development on the archegoniophore of the female mutant stopped before differentiation along the apical-basal axis only under the L/D condition (Fig. 5 and Supplementary Fig. 9). As egg cell was normally produced (Fig. 4c) and fertilization occurred in the female

Mppgdh mutant (Fig. 5d), internal serine supply seemed sufficient for these processes even without serine from PPSB. As the entire paternal genome is inactivated throughout embryogenesis in *M. polymorpha*³⁵, sporophyte from *Mppgdh-3* x Tak-1 lacked functional PPSB. In liverworts, sporophyte is dependent on gametophyte for the supply of water and nutrients³⁹. It is also possible that the PPSB in maternal gametophyte where sporophyte grows is essential for sporophyte development. Taken together, the knockout of *MpPGDH* affected male gametogenesis and embryo and sporophyte development. Serine from PPSB has importance in male and female plants differently during sexual reproduction, for gametogenesis in male and embryogenesis in female, in *M. polymorpha*.

Plants require a constant supply of serine for the biosynthesis of nucleic acids, amino acids, glutathione, and lipids^{2,3}. PPSB is involved in ammonium and sulfur assimilation in *A. thaliana*^{17,38,40} therefore, it is reasonable to assume that a lack of serine from the PPSB would extensively affect metabolism in *M. polymorpha*. Our metabolome analysis identified the metabolites related to the tricarboxylic acid (TCA) cycle, such as aconitic acid, fumaric acid, and malic acid, as DAMs in *Mppgdh* mutants (Fig. 6d, g). The result was consistent with the function reported in *A. thaliana* that PPSB represents a vital branching point in the metabolic flux between serine synthesis and the TCA cycle³. Among carbohydrates, the amounts of erythulose and erythritol were greatly decreased in the *Mppgdh* mutants (Fig. 6e; Supplementary Fig. 10b, c; Supplementary Fig. 11b). In yeast, these metabolites are derived from erythrose 4-phosphate in the pentose phosphate pathway⁴¹. Although the biosynthesis pathway of these metabolites in plants is still unclear, our result suggests that the PPSB affects central carbon metabolism. The amounts of proline and glutamine were increased in the dark in the mutants (Fig. 2). The amounts of glutaconic acid and 2-aminoadipic acid, the intermediates of lysine degradation, were reduced (Fig. 6b, e and Supplementary Fig. 17a). The DAMs detected in this study were enriched in amino acid metabolism, especially alanine, aspartate and glutamate metabolism (Fig. 6d, g and Supplementary Fig. 17c), indicating that lack of the PPSB-mediated serine widely affects metabolisms of various amino acids. Serine plays an indispensable role in the metabolism of one-carbon units². One of the main outputs of one-carbon metabolism is nucleotide biosynthesis. The amount of cytidine, a component of RNA, was increased, whereas that of dihydrouracil, an intermediate in the catabolism of uracil, was reduced in both thalli and antheridial receptacles of *Mppgdh-1* (Fig. 6b, c and Fig. 7b). These detected DAMs suggest that serine from PPSB is related to nucleotide metabolism.

We clarified that the PPSB is strongly involved in lipid metabolism. Besides serving as structural components of membranes, lipids are involved as chemical messengers/signaling molecules in various developmental processes and responses to environmental stresses^{42–46}. Lipid species vary greatly among different plants. Improved analytical technologies and bioinformatics in lipidomics⁴⁷ have enabled the investigation of highly complex composition of lipids in plants. In this study, we analyzed the lipid profile of *M. polymorpha* by using our cutting-edge lipidomics platform and discussed the link between serine metabolism and lipids. Under L/D and high CO₂ conditions, lipid profiles were changed in *Mppgdh* mutants, and several DALCs were identified (Fig. 9g and Supplementary Fig. 14f). When serine was supplemented under these two conditions, the number of DALCs was greatly reduced (Fig. 9h and Supplementary Fig. 14h), indicating that lack of serine from the phosphorylated and the glycolate pathways caused great changes in lipid profiles. Two major serine-derived lipid classes are sphingolipids and phosphatidylethanolamines (PE). Sphingolipid biosynthesis starts

from the condensation of serine with palmitoyl-CoA⁴⁸, while PE biosynthesis starts with the conversion of serine to ethanolamine⁴⁹. The contents of sphingolipids (phytosphingosine [PhytoSph], hexosylceramide hydroxyfatty acid-sphingosine [HexCer_HS], ceramide alpha-hydroxy fatty acid-phytosphingosine [Cer_AP], and ceramide non-hydroxyfatty acid-phytosphingosine [Cer_NP]) significantly decreased in *Mppgdh* mutants only under high CO₂ conditions (Fig. 9g and Supplementary Fig. 14f). PE was also reduced in thalli of male mutant under ambient CO₂ but accumulated in antheridiophores (Fig. 8c, f). Overall, our findings indicate that TCA cycle, amino acid metabolism, and nucleotide metabolism were among the primary pathways affected by serine deficiency from the PPSB. This study also revealed that lipid metabolism was affected by perturbation of serine metabolism.

The coexistence of different serine synthesis pathways complicates our understanding of the role of serine in plant development and metabolism. This study explained the specific function of PPSB in *M. polymorpha* and explored the relationship between three serine synthesis pathways in plants. Here, we present a model for functions of serine supplied by different pathways and serine homeostasis in *M. polymorpha* (Fig. 10). A large amount of serine from the photorespiratory glycolate pathway supports fundamental growth and development, and PPSB is the main pathway for serine supply at night when the glycolate pathway is inactive. Both pathways control serine homeostasis for normal growth and development. PPSB is essential for sperm and sporophyte development, and the glycolate pathway cannot fully compensate for the lack of PPSB. Serine from the glycolate pathway is sufficient for vegetative growth but not maintaining metabolic homeostasis. Lack of PPSB-derived serine triggers metabolic and lipidomic perturbation. Besides the TCA cycle, PPSB influences amino acid and nucleotide metabolism and affects lipid profiles. Serine supply solely from the glycerate pathway is insufficient for normal growth and development. Further research remains warranted to determine the possible existence of the glycerate pathway and clarify its specific function and relationship with the other two pathways. In conclusion, serine from different biosynthesis pathways has different functions in plants. This study demonstrated the importance of PPSB and serine homeostasis in growth and development.

Methods

Plant materials. We used male strain Takaragaike-1 (Tak-1) and female strain Takaragaike-2 (Tak-2) as wild types. To generate *Mppgdh* mutants using the CRISPR/Cas9 system, two gRNA sequences gRNA1 (5'-GCGCATCGTGCAAGACCGCG-3', targeting in the 1st exon) and gRNA2 (5'-TGAAGGCCGG-TAAGTGCCT-3', targeting at the junction of 1st intron and 1st exon) were designed to target *MpPGDH*. Next, the gRNA sequences were inserted into pMpGE_En03, and the gRNA expression cassette was transferred to pMpGE010⁵⁰ using LR Clonase.

To generate the lines carrying GUS reporter gene driven by the promoter of *MpPGDH* (the *proMpPGDH:GUS* lines), the genomic sequence of the upstream region of *MpPGDH* (5000 bp) was amplified with PCR using the genomic DNA of Tak-1 as a template. Subsequently, the PCR product was ligated into pMpGWB104⁵¹ to construct a pMpGWB104:*proMpPGDH* plasmid.

All plasmids were purified using LaboPass™ Plasmid Mini. The vectors (pMpGE010-*MpPGDH*-gRNA1, pMpGE010-*MpPGDH*-gRNA2, and pMpGWB104:*proMpPGDH*) were introduced into sporelings produced by crossing Tak-1 and Tak-2 via

co-cultivation with an *Agrobacterium* strain harboring the vectors. The detailed transformation method is as previously described⁵². After screening independent T₁ plants following an antibiotic selection step, we obtained 3–5 candidate lines for each plasmid in the male and female backgrounds selected via PCR using rbm27-F/rbm27-R and rhf73-F/rhf73-R, respectively⁵³. All primers used are listed in Supplementary Table 1.

Growth conditions. Wild-type and mutant *M. polymorpha* were cultivated on half-strength Gamborg's B5 medium (pH = 5.5–5.6) containing 1% agar with or without 10 mM serine at 22 °C. We used three chambers, CL with air, 16-h light/8-h dark with air, and 16-h light/8-h dark with 3000 ppm CO₂, to grow plants. To induce reproduction branches, we applied additional far-red light irradiation to each chamber. Nylon membranes were tiled onto the surface of the medium to ease the transfer of *M. polymorpha* from the agar medium.

Genetic crosses of *M. polymorpha* were performed under L/D and CL conditions as the video showed (<https://www.youtube.com/watch?v=YFjfgR-wsy0>). After male and female lines developed reproduction branches (approximately 1.5-month under L/D conditions, 1-month under CL conditions, and 2-month under L/D conditions in high CO₂), 50 µL of water was dropped on the surface of an antheridiophore (Stage 4) and left for 10 min. After pipetting five times, all water with sperm cells inside was taken and put to an immature archegoniophore. Post fertilization, 3–4 weeks were required to obtain mature sporangia that contain spores.

Western blot analysis of PGDH. Total protein from thalli of *M. polymorpha* was extracted in the sodium dodecyl sulfate (SDS) sample solution [2% (w/v) SDS, 62.5 mM Tris-HCl (pH = 6.8), 7.5% (v/v) glycerol, and 0.01% bromophenol blue]. After boiling for 5 min, the homogenate was centrifuged at 20,000 × *g* for 10 min, and the resulting supernatant was used as the protein sample. The protein concentration was determined using a BCA protein assay (Pierce). Equal amounts of proteins were separated using SDS polyacrylamide gel electrophoresis, and then transferred onto a polyvinylidene difluoride membrane. A PGDH antibody prepared using the recombinant *Arabidopsis* PGDH1 protein as the antigen⁵⁴ was used at a 1:8000 dilution. Anti-Rabbit IgG, HRP-Linked F(ab')₂ Fragment Donkey (Cytiva) was used as secondary antibody at a dilution of 1: 100,000. Chemiluminescence was used for detection of horseradish peroxidase-conjugated secondary antibodies and visualized using LAS-3000 (Fujifilm). Uncropped blots are provided in Supplementary Fig. 18.

Reverse transcription-quantitative PCR. Total RNA was extracted from the thalli and antheridial receptacles using ISO-SPIN Plant RNA (NIPPON GENE). Next, total RNA (500 ng) was reverse-transcribed using ReverTra AceTM qPCR RT Master Mix with gDNA Remover (TOYOBO). Quantitative real-time PCR was performed using THUNDERBIRDTM SYBR qPCR Mix (TOYOBO) in the StepOnePlus Real-Time PCR System (Applied Biosystems). The PCR cycling conditions were 95 °C for 15 min, 40 cycles of 95 °C for 15 s, and 60 °C for 60 s. The gene expression level was normalized to that of *MpACT1* to obtain a relative expression level.

The biological samples were analyzed in triplicate. Primers used for qPCR are listed in Supplementary Table 2.

Hoechst staining of sperm cells. Stage 4 antheridiophores were used to assess sperm production³⁶. First, 50 µL water was dropped onto the surface of each antheridiophore and left for 10 min. After pipetting five times, 30 µL water was placed in a 1.5-mL

tube with 1.5 µL bisBenzimide H33342 trihydrochloride (1 mg/mL) (Sigma-Aldrich). After staining for 10 min, 10 µL solution was drawn to a C-Chip (NanoEnTek) to check fluorescence by confocal microscopy (OLYMPUS U-HGLGPS BX53).

GUS histochemical assay. The gemmae, thalli, antheridiophores, and archegoniophores of *proMpPGDH:GUS* lines were submerged in cold 90% acetone for at least 10 min. Next, the samples were washed twice with 50 mM sodium-phosphate buffer (pH = 7.0). Subsequently, the samples were transferred into 2 mL Eppendorf tubes or 25 mL centrifuge tube (VIOLAMP) with GUS staining buffer [50 mM Na-phosphate buffer (pH7.0), 0.1% Triton, 10 mM EDTA, 0.5 mM K₃Fe(CN)₆, 0.5 mM K₄Fe(CN)₆, 1 mM X-gluc (5-bromo-4-chloro-3-indolyl-β-D-glucuronide cyclohexylammonium salt)] and incubated at 37 °C under dark conditions (for approximately 16 h). Afterward, the stained samples were decolorized and fixed in 70% ethanol overnight at 4 °C to remove chlorophyll and other plant pigments. Lastly, before observation under dissecting or light microscope (LEICA DFC450 C), the thalli were soaked in a solution [8 g choral hydrate: 3 mL water: 1 mL triglyceride] for 24 h to make them transparent.

Electron microscopy of resin-embedded tissues and surface structure. The samples were fixed with 4% paraformaldehyde and 2% glutaraldehyde in 50 mM sodium cacodylate buffer (pH = 7.4) for 2 h at 22 °C and overnight at 4 °C, then post-fixed with 1% osmium tetroxide in 50 mM cacodylate buffer for 3 h at room temperature. After dehydration in a graded methanol series (25, 50, 75, 90, and 100%), the samples were embedded in Epon812 resin (TAAB). Subsequently, ultrathin sections (100 nm) were cut using a diamond knife on an ultramicrotome (Leica EM UC7, Leica Microsystems, Germany) and placed on a glass slide. Afterward, the sections were stained with 0.4% uranyl acetate, followed by lead citrate solution, and coated with osmium using an osmium coater (HPC-1SW, Vacuum Device, Japan)⁵⁵. The coated sections were observed using FE-SEM (SU8220, Hitachi High-Tech, Japan) with a yttrium aluminum garnet backscattered electron detector at an accelerating voltage of 5 kV.

The uncoated samples were observed and imaged with a low-vacuum tabletop SEM (Hitachi TM3000, Japan) using back-scattered electrons and an accelerating voltage of 15 kV.

Preparation and observation of histological sections. For the histological cross-sections, archegoniophore and antheridiophore were dissected and fixed overnight in formalin-acetic acid-alcohol (4% formalin, 5% acetic acid, 50% ethanol) at room temperature. Then, samples were dehydrated using a graded series of ethanol washes [50, 60, 70, 80, 90, and 95% (v/v); 60 min each] and stored overnight in 99.5% (v/v) ethanol at room temperature. Next, fixed specimens were embedded in Technovit resin (Kulzer), in accordance with the manufacturer's instructions, and sectioned using a microtome (RM2125 RTS; Leica Microsystems). Sections were stained with Toluidine Blue and photographed under a microscope (Leica DM6 B) connected to a CCD camera (DFC 7000 T; Leica Microsystems).

Amino acid analysis by gas chromatography mass spectrometry. Free amino acids were extracted from 4 mg of a freeze-dried powder sample in 1 mL of extraction solvent (methanol: Milli-Q water = 4:1) placed in 2 mL sampling tubes containing 3 mm zirconia beads using a tube rotator for 10 min. After centrifugation at 14,000 rpm at 22 °C for 10 min, 900 µL of supernatant was transferred to another tube. Next, the amino acids were extracted from the residues three more times, and the four

extracted solutions were mixed. The 25 μg ^{13}C -labeled amino acids (Cambridge Isotope Laboratories) in 3.6 mL extracted solution were derivatized using the EZ: faast™ for free amino acid analysis using GC-MS (Phenomenex). Afterward, 1 μL of the solution was injected using an AOC-20i auto-injector and subjected to amino acid analysis using GCMS-QP2010 Plus (Shimadzu Corporation). The absolute concentrations of the amino acids were calculated based on those of ^{13}C -labeled amino acids.

Widely targeted metabolome analysis using gas chromatography–triple quadrupole mass spectrometry (GC-QqQ-MS). For widely targeted metabolome analysis using GC-QqQ-MS, a 4 mg freeze-dried powder sample was mixed with 1 mL extraction solvent (80% methanol and 0.1% formic acid) in 2 mL sampling tubes containing 3 mm zirconia beads on Shake Master Neo (BMS, Tokyo, Japan). After centrifugation at 100,000 rpm at 22 °C for 1 min, 200 μL of supernatant was transferred to 1.5 mL tubes containing 200 μL extraction solvent and 20 μL adonitol (0.2 mg/mL). Three blank controls (extraction solvent) and 20 quality control (QC) samples (mixed test samples) were also prepared. After vortexing, the solvents in the tubes were evaporated using a rotary evaporator (Thermo Scientific, Savant, SPD121P, & UVS800DDA) for 3 h, following which 100 μL MOX reagent (2% methoxyamine-HCl in pyridine) was added to tubes to dissolve the samples at 30 °C and 1,200 rpm for 6 h. Subsequently, 50 μL MSTFA 1% TMCS (Thermo) was added to the tubes and incubated at 37 °C and 1200 rpm for 30 min. After centrifugation at 5000 rpm for 1 min, 50 μL supernatant was collected and analyzed using GC-QqQ-MS (AOC-5000 Plus with GCMS-TQ8040, Shimadzu Corporation). All samples were tested in random order. Two QC samples were injected at regular intervals (every six test samples) throughout the analytical run for continuous recalibration. Raw data were collected using GCMS solution software (Shimadzu Corporation). Lastly, quality-filtered metabolites were selected with signal-to-noise ratio >3 and QC relative standard deviation <30%. Calculation and normalization of peak area values were conducted using MRMPROBS and LOWESS/Spline normalization tools⁵⁶. GC-MS/MS parameters⁵⁷ and MRM transitions⁵⁸ were used for widely targeted analysis.

Lipidome analysis using liquid chromatography–quadrupole time-of-flight mass spectrometry (LC-QTOF-MS). Five mg of freeze-dried powder samples were placed in a 2 mL centrifuge tube, mixed with an 800 μL of extraction solution (methyl tert-butyl ether/methanol = 3/1 (v/v) containing 1 μM of 1,2-didecanoyl-sn-glycero-3-phosphocholine, Sigma-Aldrich), and extracted by shaking at 900 rpm at 4 °C for 5 min on Shake Master Neo (BMS, Tokyo, Japan) using zirconia beads. Subsequently, 250 μL of water was added to the homogenate. After vigorous stirring on a vortex mixer and dark incubation for 15 min on ice, the homogenate was centrifuged at 1000 $\times g$ for 5 min. Afterward, the 200 μL of upper layer was transferred to a new 1.5 mL microcentrifuge tube. Next, the organic phase was evaporated to dryness using a centrifugal concentrator (ThermoSavant SPD2010, Thermo Fisher Scientific) at room temperature. The residue was dissolved in 250 μL of ethanol and centrifuged at 10,000 $\times g$ for 15 min. The supernatant was subjected to LC-MS/MS analysis⁵⁸. The dataset was analyzed using MS-DIAL version 4.80⁴⁷. The data processing parameters of minimum amplitude (for peak picking) and retention time tolerance (for peak alignment) were set to 100 and 0.1 min, respectively; however, the default parameters were used for the others. The annotation results were manually curated by considering the basis of the equivalent carbon number model of lipids, in which the elution behavior of molecules in reverse phase LC depends on the length of acyl

chains and the number of double bonds in lipids⁵⁹. The representative adduct form used for lipid quantification was determined by different polarity MS data. Lastly, the peak height was used for lipid quantification, and the total amount of each lipid class (including lipids with different acyl chains) was calculated and used for further analysis. Lipid abbreviations are listed in Supplementary Table 3.

Statistics and reproducibility. Volcano plots, Heatmaps, and KEGG pathway analysis were performed at MetaboAnalyst 5.0 (<https://www.metaboanalyst.ca/home.xhtml>). Venn diagrams were created by Webtools (<https://bioinformatics.psb.ugent.be/webtools/Venn/>). GC-QqQ-MS dataset was analyzed using MRMPROBS (<http://prime.psc.riken.jp/compms/mrmprobs/main.html>), and LC-QTOF-MS dataset was analyzed using MS-DIAL version 4.80 (<http://prime.psc.riken.jp/compms/msdial/main.html>). Principal component analysis and significance test were performed in GraphPad Prism9.0 (<https://www.graphpad.com/>). Comparisons between two groups were analyzed with unpaired *t* tests. Comparisons between two groups or more were analyzed with one-way ANOVA, and significant main effects were followed up with Tukey's multiple comparisons tests. Data are reported as mean \pm SD for column graphs and line charts. A *p*-value less than 0.05 or 0.01 was considered statistically significant. In volcano plots, *p* < 0.01 and fold change > 2 was set to identify increased metabolites, while *p* < 0.01 and fold change < 0.5 for decreased metabolites in mutants comparing with wild types. Data from this paper was collected from 3–11 biological replicates from each independent line. All figures were optimized by GraphPad Prism9.0. Exact details are listed in figure legends.

Reporting summary. Further information on research design is available in the Nature Portfolio Reporting Summary linked to this article.

Data availability

The metabolome and lipidome data were deposited into DROP Met (http://prime.psc.riken.jp/menta.cgi/prime/drop_index) under accession number DM0052. Sequence data are available from the MarpolBase (<https://marchantia.info/>) under the following accession numbers: MpPGDH (Mp8g16970), MpACT1 (Mp6g10990), MpPSAT (Mp1g15430), MpPSP (Mp2g10500), MpSHMT (Mp1g09830), MpGDH (Mp2g07580), MpDUO1 (Mp1g13010), MpDAZ1 (Mp4g11380), MpMID (Mp1g11830), MpRKD (Mp3g04030), MpPRM (Mp3g14390), MpTUA5 (Mp4g08430), MpLC7 (Mp6g01560), MpCEN1 (Mp1g00710), MpHMGBOX1 (Mp8g07450), MpHMGBOX2 (Mp2g12330), MpHMGBOX3 (Mp8g16760), MpHMGBOX4 (Mp2g04030), MpHMGBOX5 (Mp7g16870), MpTOP1 (Mp6g05370), MpTOP2 (Mp3g13420), MpTOP3 α (Mp1g02630), MpTOP3 β (Mp1g10070), MpATG5 (Mp1g12840), MpATG7 (Mp2g07850), MpATG13 (Mp7g03210). The numerical source data underlying the graphs are provided as Supplementary Data 2.

Received: 3 April 2023; Accepted: 27 December 2023;

Published online: 24 January 2024

References

1. Winter, H., Lohaus, G. & Heldt, H. W. Phloem transport of amino acids in relation to their cytosolic levels in barley leaves. *Plant Physiol.* **99**, 996–1004 (1992).
2. Kalhan, S. C. & Hanson, R. W. Resurgence of serine: an often neglected but indispensable amino acid. *J. Biol. Chem.* **287**, 19786–19791 (2012).
3. Ros, R., Muñoz-Bertomeu, J. & Krueger, S. Serine in plants: biosynthesis, metabolism, and functions. *Trends Plant Sci.* **19**, 564–569 (2014).
4. Ho, C.-L. & Saito, K. Molecular biology of the plastidic phosphorylated serine biosynthetic pathway in *Arabidopsis thaliana*. *Amino Acids* **20**, 243–259 (2001).
5. Kleczkowski, L. A. & Givan, C. V. Serine formation in leaves by mechanisms other than the glycolate. *Pathw. J. Plant Physiol.* **132**, 641–652 (1988).

6. Bauwe, H., Hagemann, M. & Fernie, A. R. Photorespiration: players, partners and origin. *Trends Plant Sci.* **15**, 330–336 (2010).
7. Maurino, V. G. & Peterhansel, C. Photorespiration: current status and approaches for metabolic engineering. *Curr. Opin. Plant Biol.* **13**, 248–255 (2010).
8. Douce, R., Bourguignon, J., Neuburger, M. & Rébeillé, F. The glycine decarboxylase system: a fascinating complex. *Trends Plant Sci.* **6**, 167–176 (2001).
9. Ros, R. et al. Serine biosynthesis by photorespiratory and non-photorespiratory pathways: an interesting interplay with unknown regulatory networks. *Plant Biol.* **15**, 707–712 (2013).
10. Servaites, J. C. & Ogren, W. L. Chemical inhibition of the glycolate pathway in soybean leaf cells. *Plant Physiol.* **60**, 461–466 (1977).
11. Randall, D. D., Tolbert, N. E. & Gremel, D. 3-phosphoglycerate phosphatase in plants. *Plant Physiol.* **48**, 480–487 (1971).
12. Kleczkowski, L. A. & Randall, D. D. Purification and characterization of a novel NADPH(NADH)-dependent hydroxypyruvate reductase from spinach leaves. Comparison of immunological properties of leaf hydroxypyruvate reductases. *Biochem. J.* **250**, 145–152 (1988).
13. Timm, S. et al. The hydroxypyruvate-reducing system in arabidopsis: multiple enzymes for the same end. *Plant Physiol.* **155**, 694–705 (2011).
14. Ho, C.-L., Noji, M. & Saito, K. Plastidic pathway of serine biosynthesis. *J. Biol. Chem.* **274**, 11007–11012 (1999).
15. Ho, C.-L., Noji, M., Saito, M., Yamazaki, M. & Saito, K. Molecular characterization of plastidic phosphoserine aminotransferase in serine biosynthesis from Arabidopsis. *Plant J.* **16**, 443–452 (1998).
16. Fell, D. A. & Snell, K. Control analysis of mammalian serine biosynthesis. Feedback inhibition on the final step. *Biochem. J.* **256**, 97–101 (1988).
17. Benstein, R. M. et al. Arabidopsis phosphoglycerate dehydrogenase1 of the phosphoserine pathway is essential for development and required for ammonium assimilation and tryptophan biosynthesis. *Plant Cell* **25**, 5011–5029 (2013).
18. Cascales-Minana, B. et al. The phosphorylated pathway of serine biosynthesis is essential both for male gametophyte and embryo development and for root growth in arabidopsis. *Plant Cell* **25**, 2084–2101 (2013).
19. Toujani, W. et al. Functional characterization of the plastidial 3-phosphoglycerate dehydrogenase family in arabidopsis. *Plant Physiol.* **163**, 1164–1178 (2013).
20. Waditee, R. et al. Metabolic engineering for betaine accumulation in microbes and plants. *J. Biol. Chem.* **282**, 34185–34193 (2007).
21. Igamberdiev, A. U. & Kleczkowski, L. A. The glycerate and phosphorylated pathways of serine synthesis in plants: the branches of plant glycolysis linking carbon and nitrogen metabolism. *Front. Plant Sci.* **9** (2018).
22. Pagnussat, G. C. Genetic and molecular identification of genes required for female gametophyte development and function in Arabidopsis. *Development* **132**, 603–614 (2005).
23. Casatejada-Anchel, R. et al. Phosphoglycerate dehydrogenase genes differentially affect Arabidopsis metabolism and development. *Plant Sci.* **306**, 110863 (2021).
24. Wang, B. et al. Characterization and expression profile analysis of the 3-phosphoglycerate dehydrogenase family in rice. *Agron. J.* **113**, 1039–1049 (2021).
25. Okamura, E. et al. Diversified amino acid-mediated allosteric regulation of phosphoglycerate dehydrogenase for serine biosynthesis in land plants. *Biochem. J.* **478**, 2217–2232 (2021).
26. Okamura, E. & Hirai, M. Y. Novel regulatory mechanism of serine biosynthesis associated with 3-phosphoglycerate dehydrogenase in Arabidopsis thaliana. *Sci. Rep.* **7**, 3533 (2017).
27. Akashi, H., Okamura, E., Nishihama, R., Kohchi, T. & Hirai, M. Y. Identification and biochemical characterization of the serine biosynthetic enzyme 3-phosphoglycerate dehydrogenase in marchantia polymorpha. *Front. Plant Sci.* **9** (2018).
28. Yoshikawa, M. et al. Wounding stress induces phenylalanine ammonia lyases, leading to the accumulation of phenylpropanoids in the model liverwort Marchantia polymorpha. *Phytochemistry* **155**, 30–36 (2018).
29. Mecchia, M. A. et al. The single Marchantia polymorpha FERONIA homolog reveals an ancestral role in regulating cellular expansion and integrity. *Development* **149** (2022).
30. Tsuzuki, M. et al. An early arising role of the MicroRNA156/529-SPL module in reproductive development revealed by the liverwort marchantia polymorpha. *Curr. Biol.* **29**, 3307–3314.e5 (2019).
31. Higo, A. et al. Transcription factor DUO1 generated by neo-functionalization is associated with evolution of sperm differentiation in plants. *Nat. Commun.* **9**, 5283 (2018).
32. Hisanaga, T. et al. Building new insights in plant gametogenesis from an evolutionary perspective. *Nat. Plants* **5**, 663–669 (2019).
33. Norizuki, T., Minamino, N., Sato, M., Tsukaya, H. & Ueda, T. Dynamic rearrangement and autophagic degradation of mitochondria during spermiogenesis in the liverwort Marchantia polymorpha. *Cell Rep.* **39**, 110975 (2022).
34. Rövekamp, M., Bowman, J. L. & Grossniklaus, U. Marchantia MpRKD regulates the gametophyte-sporophyte transition by keeping egg cells quiescent in the absence of fertilization. *Curr. Biol.* **26**, 1782–1789 (2016).
35. Montgomery, S. A. et al. Polycomb-mediated repression of paternal chromosomes maintains haploid dosage in diploid embryos of Marchantia. *Elife* **11** (2022).
36. Higo, A. et al. Transcriptional framework of male gametogenesis in the liverwort marchantia polymorpha L. *Plant Cell Physiol.* **57**, 325–338 (2016).
37. Kawamura, S. et al. MarpolBase Expression: a web-based, comprehensive platform for visualization and analysis of transcriptomes in the liverwort marchantia polymorpha. *Plant Cell Physiol.* **63**, 1745–1755 (2022).
38. Zimmermann, S. E. et al. The phosphorylated pathway of serine biosynthesis links plant growth with nitrogen metabolism. *Plant Physiol.* **186**, 1487–1506 (2021).
39. Raven, J. A. Long-distance transport in non-vascular plants. *Plant. Cell Environ.* **26**, 73–85 (2003).
40. Anoman, A. D. et al. Deficiency in the phosphorylated pathway of serine biosynthesis perturbs sulfur assimilation. *Plant Physiol.* **180**, 153–170 (2019).
41. Wang, N. et al. Metabolic engineering of Yarrowia lipolytica for thermoresistance and enhanced erythritol productivity. *Biotechnol. Biofuels* **13**, 176 (2020).
42. Wolters-Arts, M., Lush, W. M. & Mariani, C. Lipids are required for directional pollen-tube growth. *Nature* **392**, 818–821 (1998).
43. Wang, Y.-S., Yao, H.-Y. & Xue, H.-W. Lipidomic profiling analysis reveals the dynamics of phospholipid molecules in Arabidopsis thaliana seedling growth. *J. Integr. Plant Biol.* **58**, 890–902 (2016).
44. Welti, R. Plant lipidomics: Discerning biological function by profiling plant complex lipids using mass spectrometry. *Front. Biosci.* **12**, 2494 (2007).
45. Wang, X. & Chapman, K. D. Lipid signaling in plants. *Front. Plant Sci.* **4** (2013).
46. Cheong, B. E. et al. Phenotyping the chilling and freezing responses of young microspore stage wheat spikes using targeted metabolome and lipidome profiling. *Cells* **9**, 1309 (2020).
47. Tsugawa, H. et al. A lipidome atlas in MS-DIAL 4. *Nat. Biotechnol.* **38**, 1159–1163 (2020).
48. Teng, C. et al. Serine palmitoyltransferase, a key enzyme for de novo synthesis of sphingolipids, is essential for male gametophyte development in Arabidopsis. *Plant Physiol.* **146**, 1322–1332 (2008).
49. Liu, Y., Gunawan, F., Yunus, I. S. & Nakamura, Y. Arabidopsis serine decarboxylase 1 (SDC1) in phospholipid and amino acid metabolism. *Front. Plant Sci.* **9** (2018).
50. Sugano, S. S. et al. Efficient CRISPR/Cas9-based genome editing and its application to conditional genetic analysis in Marchantia polymorpha. *PLoS One* **13**, e0205117 (2018).
51. Ishizaki, K. et al. Development of gateway binary vector series with four different selection markers for the liverwort marchantia polymorpha. *PLoS One* **10**, e0138876 (2015).
52. Tsuboyama, S. & Kodama, Y. AgarTrap: a simplified agrobacterium-mediated transformation method for sporelings of the liverwort marchantia polymorpha L. *Plant Cell Physiol.* **55**, 229–236 (2014).
53. Fujisawa, M. et al. Isolation of X and Y chromosome-specific DNA markers from a liverwort, marchantia polymorpha, by representational difference analysis. *Genetics* **159**, 981 LP–981985 (2001).
54. Yoshida, K., Ohtaka, K., Hirai, M. Y. & Hisabori, T. Biochemical insight into redox regulation of plastidial 3-phosphoglycerate dehydrogenase from Arabidopsis. *Thalassia. J. Biol. Chem.* **295**, 14906–14915 (2020).
55. Hiwatashi, T. et al. The RopGEF KARAPPO is essential for the initiation of vegetative reproduction in marchantia polymorpha. *Curr. Biol.* **29**, 3525–3531.e7 (2019).
56. Tsugawa, H., Kanazawa, M., Ogiwara, A. & Arita, M. MRMPROBS suite for metabolomics using large-scale MRM assays. *Bioinformatics* **30**, 2379–2380 (2014).
57. Tabeta, H. et al. An auxin signaling network translates low-sugar-state input into compensated cell enlargement in the fugu5 cotyledon. *PLOS Genet.* **17**, e1009674 (2021).
58. Tabeta, H. et al. Skotomorphogenesis exploits threonine to promote hypocotyl elongation. *Quant. Plant Biol.* **3**, e26 (2022).
59. Tsugawa, H. et al. A cheminformatics approach to characterize metabolomes in stable-isotope-labeled organisms. *Nat. Methods* **16**, 295–298 (2019).

Acknowledgements

We greatly appreciate Drs. Mie Shimojima (Tokyo Institute of Technology) and Hiroyuki Imai (Konan University) for discussion on lipids, Mr. Kouji Takano (RIKEN Center for Sustainable Resource Science) for his help on preparing LC-MS/MS samples, Dr. Hideya Fukuzawa (Kyoto University) for his assistance with high CO₂ experiments, Ms. Yoriko Matsuda (Kyoto University) for her technical assistance with construction of CRISPR/Cas9 lines, Ms. Junko Takanobu (RIKEN Center for Sustainable Resource Science) for her help in preparing culture medium and weighing samples, and Dr. Takashi Araki

(Kyoto University) for his useful advice in interpretation of the results about male gametogenesis. We are grateful to Graduate Program of Transformative Chem-Bio Research (GTR) program in Nagoya University to support this study. This work was supported in part by JSPS KAKENHI Grant Numbers 25113010 and 20H04852, and GteX Program Japan Grant Number JPMJGX23B0 to M.Y.H.

Author contributions

M.Y.H. conceived the idea for the project. M.Wang prepared the draft. M.Wang, H.Tabeta., and K.O. checked the growth and development phenotypes, including thalli growth, sperm production, and spore formation. M.Wang conducted GUS staining experiments and prepared samples for metabolic and lipidomic analysis. H.Tabeta. performed metabolic analysis and cross-section microscopic analyses. A.K. measured free amino acid contents. K.T., M.S., and M.Wakazaki performed the FE-SEM analyses. H.Tusgawa., T.S., and Y.O. performed lipidomic analysis. H.Tsugawa, T.I., M.Wang and M.Y.H. discussed lipidome annotation. H.A., T.K., R.N., and K.Y. supported the construction of *Mppgdh* mutants and GUS lines. K.Y. performed western blot experiment. M.Wang, H.Tabeta., R.S., A.F., and M.Y.H. discussed the results and wrote the manuscript.

Competing interests

The authors declare no competing interests.

Additional information

Supplementary information The online version contains supplementary material available at <https://doi.org/10.1038/s42003-023-05746-6>.

Correspondence and requests for materials should be addressed to Masami Yokota Hirai.

Peer review information *Communications Biology* thanks Roc Ros, Zhong-Hua Chen, and the other, anonymous, reviewer(s) for their contribution to the peer review of this work. Primary Handling Editor: George Inglis. A peer review file is available.

Reprints and permission information is available at <http://www.nature.com/reprints>

Publisher's note Springer Nature remains neutral with regard to jurisdictional claims in published maps and institutional affiliations.



Open Access This article is licensed under a Creative Commons Attribution 4.0 International License, which permits use, sharing, adaptation, distribution and reproduction in any medium or format, as long as you give appropriate credit to the original author(s) and the source, provide a link to the Creative Commons license, and indicate if changes were made. The images or other third party material in this article are included in the article's Creative Commons license, unless indicated otherwise in a credit line to the material. If material is not included in the article's Creative Commons license and your intended use is not permitted by statutory regulation or exceeds the permitted use, you will need to obtain permission directly from the copyright holder. To view a copy of this license, visit <http://creativecommons.org/licenses/by/4.0/>.

© The Author(s) 2024